GEOCHEMICAL MAPPING BY UNMIXING ALLUVIAL SEDIMENTS: AN EXAMPLE FROM NORTHERN AUSTRALIA

SUBMITTED, NON-PEER REVIEWED MANUSCRIPT, COMPILED OCTOBER 2, 2022

Alex G. Lipp[1*], **Patrice de Caritat**[2], **and Gareth G. Roberts**[1]

[1]Department of Earth Sciences and Engineering, Imperial College London, UK
[2]Geoscience Australia, Canberra, Australia

Manuscript submitted for publication in *Journal of Geochemical Exploration*

Preprint doi: 10.31223/X5ZM09

ABSTRACT

Alluvial sediments have long been used in geochemical surveys as their compositions are assumed to be representative of areas upstream. Overbank and floodplain sediments, in particular, are increasingly used for regional to continental-scale geochemical mapping. However, during downstream transport, sediments from heterogeneous source regions are carried away from their source regions and mixed. Consequently, using alluvial sedimentary geochemical data to generate continuous geochemical maps remains challenging. In this study we demonstrate a technique that numerically unmixes alluvial sediments to make a geochemical map of their upstream catchments. The unmixing approach uses a model that predicts the concentration of elements in downstream sediments, given a map of the drainage network and element concentrations in the source region. To unmix sedimentary chemistry, we seek the upstream geochemical map that, when mixed downstream, best fits geochemical observations downstream. To prevent overfitting we penalise the roughness of the geochemical model. To demonstrate our approach we apply it to alluvial samples gathered as part of the Northern Australia Geochemical Survey. This suvey gathered samples collected over a ~ 500,000 km^2 area in northern Australia. We first validate our approach for this sample distribution with synthetic tests, which indicate that we can resolve geochemical variability at scales greater than 0.5 – 1° in size. We proceed to invert real geochemical data from the total digestion of fine-grained fraction of alluvial sediments. The resulting geochemical maps for two elements of potential economic interest, Cu and Nd, are evaluated in detail. We find that in both cases, our predicted downstream concentrations match well against a held-out, previously 'unseen' subset of the data, as well as against data from an independent geochemical survey. By performing principal component analysis on maps generated for all 46 available elements we produce a synthesis map to identify the significant geochemical domains in this part of northern Australia. This map shows strong spatial similarities to the underlying lithological map of the area. Finally, we compare the results from our approach to a geochemical map produced by kriging. We find that, unlike the method presented here, kriging generates geochemical maps that are both dampened relative to expected magnitude, as well as being spatially distorted. We argue that the unmixing approach is the most appropriate method for generating geochemical maps from regional-scale alluvial surveys.

***K*eywords** Geochemical Mapping · Catchment sediments · Inverse Modelling · Unmixing · Northern Australia · Geochemical Survey · National Geochemical Survey of Australia

1 INTRODUCTION

1.1 Context

Geochemical maps are essential geoscience data products used for generating environmental baselines, identifying mineral deposits, and aiding wider geologic understanding (Garrett et al. 2008). There is a growing demand for geochemical maps that cover continental areas, and eventually, the whole of Earth's surface. However, at present only ~ 27 % of Earth's continental surface is geochemically mapped at any scale (Wang et al. 2020). Geochemically surveying large areas remains challenging as there is a perception that large numbers of samples must be collected and analysed. Significant effort has thus been expended in developing methods to develop geochemical maps from low-density sampling campaigns (e.g., Smith and Reimann 2008; Zhao et al. 2014; Birke et al. 2015; Liu et al. 2021.) A widely used low-density approach is to sample sediments from stream, overbank or floodplain deposits. Herein we refer to all such types of sediment as alluvial sediments. Alluvial sediments are assumed to integrate their entire upstream areas and hence thought to be more representative than, say, soil samples (e.g., Ottesen et al. 1989; Xie and Cheng 1997; Bølviken et al. 2004). This approach assumes that rivers efficiently mix the components of rocks outcropping in their basins, transporting this mixture toward their outlets. Sampling of alluvial sediments has been widely used to generate geochemical maps with a range of different sampling densities on regional, national and continental scales (e.g., Johnson et al. 2005; Caritat and Cooper 2016; Bastrakov et al. 2018; Vicente et al. 2020; Wang et al. 2022).

1.2 Motivation

The alluvial sampling approach described above presents challenges for further analysis. Frequently, we wish to generate

*correspondence: `a.lipp18@imperial.ac.uk`, `alexander.lipp@merton.ox.ac.uk`

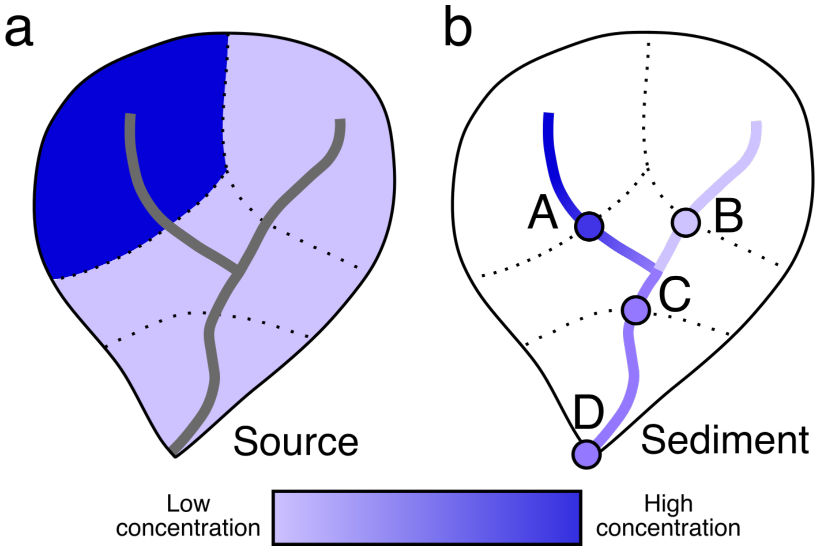

Figure 1: **Mixing heterogeneous geochemistry downstream.** a) A river (grey lines) whose drainage basin contains two lithologies which have high (dark blue) and low (light blue) concentrations of some element or tracer. b) Coloured lines indicate the composition of sediment in the river across the basin. Coloured circles indicate labelled sample localities. Sub-catchments are indicated by dotted lines. In the upstream sub-catchments (points A and B), the composition of sediment is the same as the source region (panel a). Downstream, after the confluence (i.e., at points C and D), the sediment is a mixture of the two lithologies and distinct from the source composition at the same point.

a continuous 2D map from discrete geochemical observations. Such continuous maps are essential for utilising survey data as environmental baselines and for visualisation purposes (e.g., generating products such as the Forum of European Geological Surveys atlas; Salminen et al. 2005). Additionally, subsequent data analysis, for example for prospectivity mapping or anomaly separation, may require geochemical information to be in a raster/grid format, comparable to other datasets such as topography, satellite imagery or geophysics (e.g., Rodriguez-Galiano et al. 2015). Unfortunately, generating such raster maps from alluvial point observations is challenging because typical geostatistical procedures such as kriging cannot be used without careful consideration. Kriging assumes that the underlying function is sampled directly at the observation point. Whilst this may be true for media such as soils, it is not the case for alluvial sediments which instead integrate an entire upstream area. Moreover, the actual underlying rock chemistry at the point of observation may not even be similar to the chemistry of the sediment, which will have been transported to that locality from elsewhere. This represents a challenge as in geochemical surveys we, generally, seek information about the geochemistry of the sediment's ultimate *sources* not the sediment itself. Moreover, kriging typically (but not necessarily, e.g., Kim and O'Neil 1997) makes use of the geographic distance between two samples, whereas for samples extracted on drainage networks it is the *topological* distance along flow-lines that is most relevant.

Attempts have been made to combine geochemical information of samples with the structure of the drainage network they are sampled from. The most common approach, termed the 'sample catchment basin' (SCB) approach, is based on extrapolating the measured values across the subcatchment which that sample uniquely defines, up to the next upstream sample, or the watershed (e.g., Bonham-Carter and Goodfellow 1986; Carranza and Hale 1997; Moon 1999; Spadoni et al. 2004; Spadoni 2006; Carranza 2010; Yousefi et al. 2013). However, this approach fails to resolve the issue that downstream samples are mixtures of all upstream nested subcatchments, and not just the subcatchment which it uniquely samples (as recognised in Spadoni et al. 2004).

A related problem with alluvial sediments is that they are mixtures of material originating higher up in the catchment, which, other than in the simplest case, consists of more than a single lithology. Consider for example Figure 1 which shows a drainage basin containing two geochemically distinct lithologies with differing concentrations of some tracer element. The composition of the downstream mixture sediment is shown in Figure 1b. This drainage basin is sampled at four localities, indicated as sites A–D in Figure 1b, which split the basin into sub-catchments. We seek to recover the source map in Figure 1a from these discrete observations. The SCB approach would assign the composition of the mixtures to each sub-catchment. This approach would successfully identify the composition of the upstream sub-catchments A and B. However, the approach would erroneously set the downstream portions of the basin (i.e., sub-catchments C and D) to the intermediate mixture value. Hence, the recovered source map using this approach would be inaccurate. Kriging and other interpolation methods would also produce erroneous results, failing to consider the topology of the network.

1.3 Proposed Solution

In this study we demonstrate a methodology that is able to accurately recover source region chemistry from downstream observations. Our inverse modelling approach is able to unmix the geochemistry of alluvial sediments to generate continuous maps of the source geochemistry upstream. Our approach first defines a forward model that, given a drainage map of a region, can translate geochemical maps of source regions into predictions of the geochemistry of sediments in channels downstream. We then invert the downstream observations to calculate the upstream geochemical map, that, when mixed along drainage (using the forward model), best fits a suite of geochemical observations downstream.

This approach was first proposed, and validated against independent data, in a 13,000 km^2 pilot study in the Cairngorms mountains, UK using relatively high-density (1 sample per 2 km^2) geochemical data (Lipp et al. 2021). In the present contribution we upscale this approach considerably to generate regional scale geochemical maps from a survey in northern Australia (Bastrakov et al. 2018). This survey covers a region one order of magnitude larger at a density two orders of magnitude lower.

1.4 Paper Outline

We first introduce the study area and survey in northern Australia that is used to demonstrate the methodology. Next we describe how we unmix a suite of geochemical observations to make a geochemical map. We then test the efficacy and resolution of our approach through a suite of synthetic tests. Satisfied with the results of these synthetic tests we proceed to invert the entire Northern Australia Geochemical Survey (NAGS) dataset. For brevity, the results of just two elements, copper (Cu) and neodymium (Nd), are presented here. Maps of the 44 other analysed elements are displayed in the Supplementary Information and made available as ASCII grid files (see 'Code and Data Availability' section). A synthesis geochemical map, generated by applying principal component analysis to the maps of all elements is then presented and compared to published geological maps. Finally, we compare maps generated through this unmixing approach to those generated by kriging.

1.5 Regional Setting

1.5.1 Climate and physiography

The study area encompasses the states of Queensland and Northern Territory, bounded by Gulf of Carpentaria in the north. The main climate zones in the area are described as 'Hot humid summer' in the north and along the coast, and 'Warm humid summer' further south and inland (all climate and vegetation data can be accessed from the Bureau of Meteorology, Australian Government; `www.bom.gov.au`). Average annual rainfall over the four-year period to 2017 (when sampling was carried out) mostly ranges from 400 – 900 mm/yr and is strongly seasonal (austral summer rain). Notably, the study area includes the west-northwest to east-southeast trending Barkly Tablelands Region, described as 'black clay plains, sandy rises of ferruginous sandstone, and minor stony limestone plains, interior drainage with calcrete in depressions' (Pain et al. 2011). The topography ranges from sea-level to 610 m elevation, with a mean altitude of 240 m (Figure 2a).

The dominant soil orders encountered in the study area are, according to the Australian Soil Classification scheme, tenosol, vertosol, kandosol (each representing ~ 25 % of the study area) and rudosol (20 %; Northcote et al. 1968; Isbell 2016). Landuse over the area (2001–2002) is overwhelmingly classified by the Australian Soil Resource Information System as 'Grazing natural vegetation'.

1.5.2 Geology

The study area displays a complex and protracted geological history that can be traced back to ~ 1860 Ma, with the central cratonic nucleus of the Paleo- to Mesoproterozoic North-Australian Craton being flanked by younger Proterozoic and Paleozoic orogenic belts and basins, including the Phanerozoic Tasmanides to the east (Ollier 1988; Braun et al. 1998; Betts et al. 2002; Blewett 2012; Withnall et al. 2012; Ahmad and Scrimgeour 2013; Clark et al. 2022). Mesozoic and Cenozoic sedimentary sequences of the Eromanga and Carpentaria basins conceal much of the basement terrain over the eastern part of the study area (Figure 2b). The whole region has experienced extensive weathering resulting in a ubiquitous and locally thick mantle of regolith.

1.5.3 Mineral occurrences

Numerous mineral occurrences are found in northern Australia, including 128 'mineral deposits' (discovered but not exploited) and 'operating mines' (producing) reported by Senior et al. (2021) within the NAGS study area (Figure S1 in Supplementary Information). These are mainly base metal (Pb, Zn, and Cu), but also include battery alloys (Ni, Co, Mn, V, Mo, Mg), fertiliser (P, K), iron ore, precious metal (Au, Ag) and U occurrences. Though many of these 128 occurrences are small, five Tier 1 occurrences are found within the study area: the George Fisher Pb-Zn mine, Mount Isa Pb-Zn deposit, and McArthur River Pb-Zn mine (all > 20 Mt total resources, i.e., the sum of economic demonstrated, subeconomic and inferred resources), and the Mount Isa and George Fisher Ag mines (> 20 kt total resources); and a further six Tier 2 occurrences are also recorded in the area: the Woonarah phosphate, Teena Pb-Zn and Merlin diamond mineral deposits, the Mount Isa Cu mine, and the Mount Dromedary and Burke graphite mineral deposits (Table S1 in Supplementary Information). Thus the NAGS area is highly prospective and, given the ubiquity of (sedimentary) cover, remains poorly explored at depth.

1.6 Northern Australia Geochemical Survey

The Northern Australia Geochemical Survey (NAGS; Bastrakov et al. 2018) was a collaboration between Geoscience Australia, the Northern Territory Geological Survey and the Geological Survey of Queensland, which closely followed the strategies and workflows established by the earlier National Geochemical Survey of Australia (NGSA; Caritat et al. 2011; Caritat 2018) . NAGS targeted catchment outlet sediments at an average sample density of one site per ~ 500 km^2, approximately ten times that of NGSA, over a ~ 500,000 km^2 area straddling the Northern Territory-Queensland border in northern Australia. These sediments best represent well-mixed, fine-grained composite samples of major rock and soil types present in the upstream catchments. Catchment outlet sediments are similar to overbank or floodplain sediments, i.e., collected outside river channels near the outlet or spill points of catchments, but with the acknowledged potential influence of aeolian processes in many places in Australia. A total of 776 sampling sites were accessed in 2017, mostly by helicopter. On-site field sampling procedures followed those developed for the NGSA, but only the top outlet sediment (TOS; 0–10 cm depth) was sampled. Two size fractions ($< 75\ \mu$m and < 2 mm) were separated from the bulk material for each sample. Both size fractions were analysed for their elemental composition (> 50 chemical elements) by several analytical methods. Analyses were performed at the Geoscience Australia laboratories in Canberra (fused bead X-ray fluorescence—XRF, and total digestion inductively coupled plasma – mass spectrometry—ICP-MS), SGS Australia mineral services in Perth (Mobile Metal Ion$^{\text{TM}}$—MMI) and ALS laboratories in Perth (aqua regia—AR, and fire assay—FA). Two size fractions and three digestion strengths were chosen, consistent with the NGSA, to better discriminate between geochemical signatures that might result from different transport mechanisms for metals, and to emphasise contributions from mineral systems. The NAGS dataset includes (1) information on the sampling sites, (2) bulk sample properties (Munsell colours, pH and electrical conductivity), (3) partial leach multi-element analyses of the MMI extractions (< 2 mm fraction only, ICP-MS), (4) total multi-element analyses of the coarse (< 2 mm) and fine ($< 75\ \mu$m) fractions of the samples (XRF and ICP-MS), (5) AR multi-element analyses of the coarse and fine fractions, and (6) FA analysis for Au, Pt and Pd of the coarse and fine fractions. Herein only total concentrations (XRF and ICP-MS) determined on the $< 75\ \mu$m TOS samples are used.

2 METHODS

2.1 Modelling

We first consider how a given upstream geochemical map can be used to predict elemental concentrations downstream. We then show how to 'invert' this formulation to determine the best-fitting upstream geochemical map that describes a suite of observations downstream. Finally we describe how this inverse approach can be solved numerically through discretisation and optimisation methods.

We consider a map of concentrations of some arbitrary element, $C(x, y)$, continuously defined across the studied area. This map represents the *source* of sediments, which is likely controlled by the underlying lithology. We define the concentration of the same element in a downstream fluvial sediment as $D(x, y)$. Assuming conservative mixing upstream, D can be described at any location in the drainage basin simply as the area weighted integral of C over the upstream area of that point A. Hence:

$$D(x, y) = \frac{1}{|A|} \int_A C(x, y)\ \mathrm{d}A = F(C). \tag{1}$$

This forward model, which translates a map of source region concentrations into predictions of downstream chemistry, is termed F. Note that this formulation assumes that the erosion rate (i.e., the total amount of sediment that each point in the landscape produces) is homogenous. Should accurate information about spatially varying sediment production rates be known, these can easily be incorporated (e.g., see Equation 1 in Lipp et al. 2021). Note also that we do not consider any in-transit modification of sediment chemistry, e.g., from chemical weathering (Ercolani et al. 2019; Lipp et al. 2020). Whilst these assumptions are a simplification, their validity can be implicitly assessed using independent data.

2.2 Inverse modelling

We seek the upstream geochemical map C that best explains some observed downstream concentrations D_{obs}. The misfit between a given observation D_i, and a predicted concentration is defined in terms of C as:

$$\log\{F(C)_i\} - \log\{D_{obs,i}\}.$$

We use the log-ratio difference as the misfit as typically geochemical data is logarithmically distributed, and for geochemical mapping it is *relative* not absolute variations that are considered most meaningful (Grunsky 2010).

The optimal map for a suite of observations downstream will minimise the global misfit between predictions and observations: $\|\log\{F(C)_i\} - \log\{D_{obs,i}\}\|_2^2$. However, data contain random analytical and sampling error. Consequently, if only the misfit is minimised, the resulting 'optimal' C will overfit the data to recreate these random variations. To prevent this overfitting we also include a regularising term that penalises the spatial roughness of C: $\|\nabla \log\{C\}\|_2^2$. Thus, we seek C that minimises the following objective function:

$$X(\mathbf{C}) = \overbrace{\|\log\{F(C)\} - \log\{D_{obs}\}\|_2^2}^{Misfit} + \overbrace{\lambda^2 \|\nabla \log\{C\}\|_2^2}^{Regulariser} \tag{2}$$

where λ is a hyperparameter controlling the strength of smoothing. This hyperparameter is calibrated independently using the validation dataset (as discussed below).

2.3 Implementation

To minimise Equation 2 numerically we discretise C onto a square grid with resolution 0.125 degrees (~ 14 km) in both longitudinal and latitudinal directions, generating a grid that has 90 columns and 68 rows. Hence, C is approximated by the vector $\mathbf{C}$ which has length equal to the number of nodes in the inversion grid. D_{obs} is represented as the vector $\mathbf{D_{obs}}$ which is a vector containing the individual point observations gathered during the geochemical survey. Note that whilst this problem is underdetermined ($\mathbf{C}$, the variables we solve for, is longer than $\mathbf{D_{obs}}$, the number of constraints) it can be solved due to the presence of the regulariser term. The coarseness of the inversion grid is limited by computational efficiency as this affects the time taken to optimise Equation 2. Implementing faster solvers for this problem is an active line of enquiry.

Note, that we only consider inversion nodes that overlap with drainage basins containing a sample downstream. Consequently, the actual modelled domain is irregular in shape, and contains regions of no coverage where no samples were gathered (e.g., grey areas in maps below).

X, which is nonlinear and non-convex, is minimised with respect to $\mathbf{C}$ using the modified version of Powell's conjugate direction method as implemented in the `SciPy` package for `python` (Press et al. 1992; Virtanen et al. 2020). Powell's method is chosen as it does not require derivatives to be calculated.

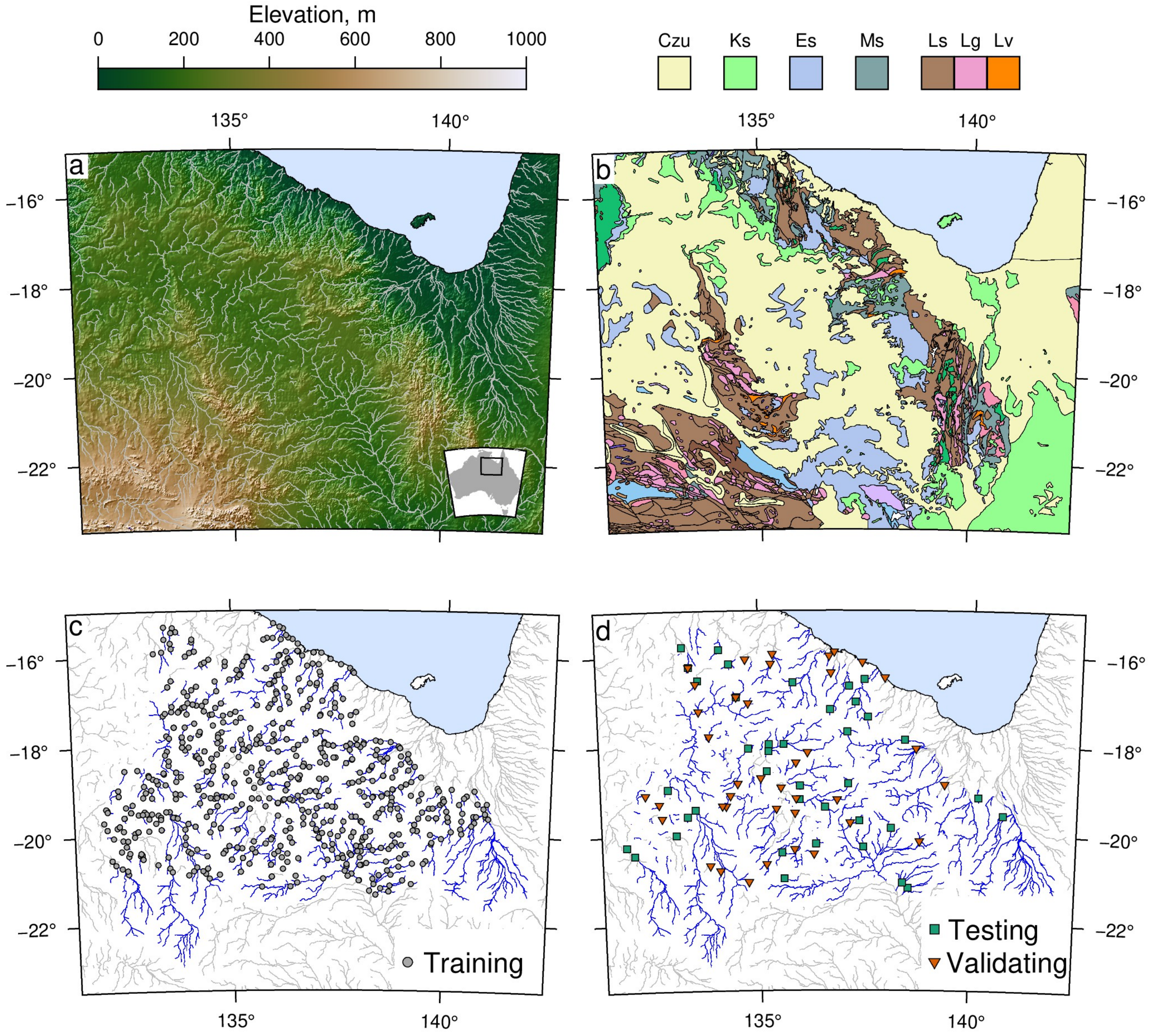

Figure 2: **Overview of study area and sample sites.** a) Topography of northern Australia overlain with channels draining catchments greater than 250 km^2 in area. Both topography and channels based on data from Hutchinson et al. (2008). Inset map shows location of study area within Australia. b) 1:1 million scale geological map of Australia (Raymond et al. 2012). Colours for selected lithologies shown: CZu = Cenozoic sediments; Ks = Cretaceous sediments; Es = Cambrian sediments; Ms = Mesoproterozoic sediments; Ls = Paleoproterozoic sediments; Lg = Paleoproterozoic felsic intrusives; Lv = Paleoproterozoic intermediate volcanics; See original source for full legend. c) Locations of NAGS samples within the training dataset. Blue lines show channels within the covered area. d) Locations of NAGS samples within the testing (green squares) and validating (orange triangles) datasets.

This use of Powell's method contrasts with Lipp et al. 2021 where the, slower, Nelder-Mead algorithm is used (Gao and Han 2012). An additional difference to the previous implementation is that the forward model has been parallelised to speed up computation time. We parallelise the forward model by performing the integral on each distinct drainage basin basin in parallel (e.g., Braun and Willett 2013).

3 Data

3.1 Sedimentary Geochemical Data

In this study we analyse the elemental concentration of the fine fraction (< 75 μm) of alluvial sediments following fusion/total digestion. Data were gathered by a combination of X-ray fluorescence (XRF) and inductively coupled plasma mass spectroscopy (ICP-MS). Subsequently, all data went through a data quality procedure removing elements that failed to consistently replicate standards. Imputation of missing and below-detection-limit values was then performed. To calculate the error, σ, on each observation we use the reported relative standard deviations calculated using field duplicates. These are then converted into logarithmic standard deviations by taking the mean of the upper and lower bounds. Full details of sampling, analytical and quality control methods are given in Bastrakov et al. (2018). Of the 47 elements that passed through this quality control procedure we analyse 46, excluding Scandium as it was found to contain large amounts of spurious variance introduced by the imputation process.

We split the 775 NAGS samples into training, validation and test datasets of 697, 39 and 39 samples respectively which approximates a 90:5:5 % split. The locations of the respective datasets are shown in Figures 2c & d. The validation dataset is used to select appropriate hyper-parameters (see below) and the test dataset is used to independently determine the accuracy of the modelled solution. Neither the test and validation datasets are used in the inversion calculations.

3.2 Drainage

To define drainage across the study area we use the GEODATA 9 arcsecond Flow Direction Grid of Australia produced by Geoscience Australia (Hutchinson et al. 2008). This flow-direction map is automatically generated from topographic data, but adjusted such that modelled streamlines align with independently determined streamlines. The modelled drainage network (with a catchment area threshold greater than 250 km^2) is displayed in Figure 2a.

The D8 method of encoding flow assumes only convergent flow, which can introduce inaccuracies in areas of divergent flow and low topographic relief (O'Callaghan and Mark 1984). This issue is most likely to be present in the region of internal drainage within the central portion of the studied region.

3.3 Aligning sample sites to drainage

Before inversion, the locations of samples must be aligned to the locations of channels on the drainage network grid. This requires care as small changes in the location of samples on the network could introduce large differences in the resulting upstream map. For example, consider the differences in interpretations from a sample gathered immediately above a major confluence to one gathered immediately below the confluence. To make sure this alignment is as accurate as possible we use the target upstream catchment polygons published alongside the NAGS dataset (Bastrakov et al. 2018). For each of the catchment polygons we identify the point within it with the largest drainage area (to access its outflow point). This step produces a suite of candidate aligned sample sites. Then, for each actual sample site we identify the nearest candidate site using the Haversine (great circle) distance. The accuracy of this alignment was assessed by visual inspection and the vast majority of samples clearly align to a nearby channel node. In the flat region to the south west with poorly defined and internal drainage, the sample sites are found to be further from a fitted channel location.

3.4 Calibrating smoothing parameter

We use the validation dataset to calibrate λ by, for each element, minimising Equation 2 for a range of different λ values. We then choose the result whose downstream predictions most closely match the validation dataset. The resulting λ against RMS plots are shown for all elements in Figure S2 and S3 in the Supplementary Information. For most elements, the relationship between λ and the validation RMS is simple with a single global minimum close to $\lambda = 10^{3.5}$ (e.g., Aluminium; Figure S2). In most cases this method of choosing λ produces sensible results with maps generally having a similar level of roughness. However, in a small number of cases the returned λ value produce geochemical maps that are significantly rougher than other maps, with the χ values indicating overfitting (e.g., Copper; Figure S2). Additionally, in some rare cases there are multiple minima (e.g., Calcium; Figure S2) or no clear minimum at all. In these cases the λ value was chosen by visual inspection such that the roughness of the solution aligned with other elements. The poorly defined minima, and the anomolous λ values are likely a result of using a relatively small validation dataset which is more influenced by outlier samples.

3.5 Projections

Figures were generated and geospatial processing performed using the Generic Mapping Tools (Wessel et al. 2019). All maps (except where indicated) use a Lambert Conformal Conic projection with standard parallels at -18 and -36°N

4 Results

4.1 Synthetic Data

We first explore whether our method is able to recover a known synthetic input. We generate a 2D sinusoidal pattern ranging from 10^2 – 10^4 mg kg^{-1} (in logarithmic space) with a spatial wavelength of 2° (Figure 3a). Applying the forward mixing model (Equation 1) to this input we generate a suite of synthetic 'observations'. To these observations we add noise equal to a relative standard error of 10 %, which is comparable to observed errors. We then apply the method described above to invert these observations for source chemistry. The recovered map is shown in Figure 3b. This test is analogous to 'chequerboard' tests carried out in seismic tomography and other geophysical inversions (e.g., Rawlinson et al. 2014).

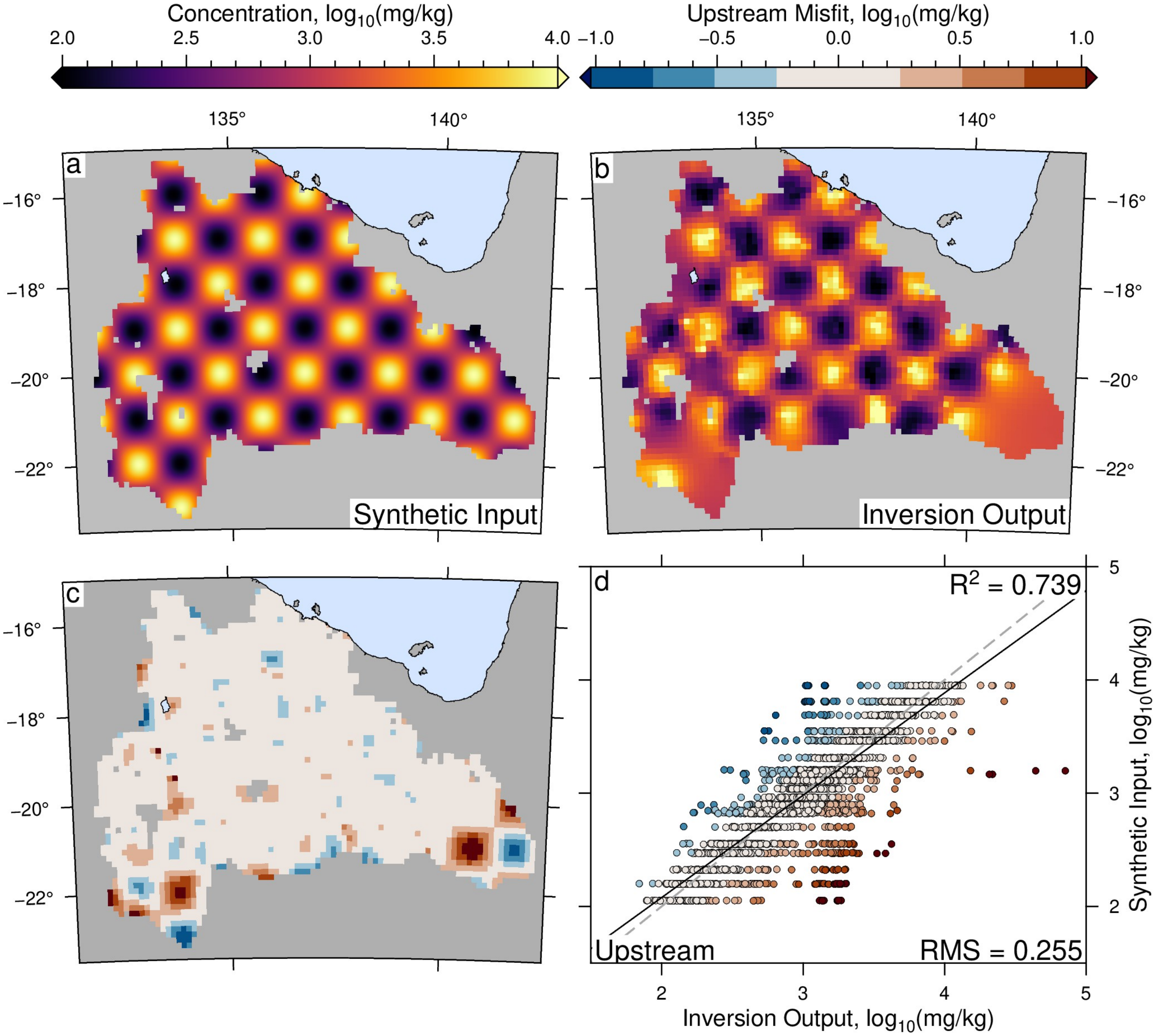

Figure 3: **Inverting synthetic data: recovering upstream source concentrations.** a) Input data used to generate synthetic downstream data. Concentration map of an arbitrary tracer which varies sinusoidally from 10^2–10^4 mg kg^{-1} with a spatial wavelength of 2°. Greyed out regions (in all maps) indicate areas outside of modelled domains. b) Recovered pattern from inverting synthetic data with 10 % noise with a smoothing factor of $10^{2.3}$ c) Misfit between recovered inversion and the initial input. Colour bar is incremented in intervals equal to the root mean square (RMS) misfit, shown in panel d. d) Cross plot between recovered map and synthetic map (downsampled to resolution of inversion). Grey dashed line = 1:1 line; solid black line = regression through data.

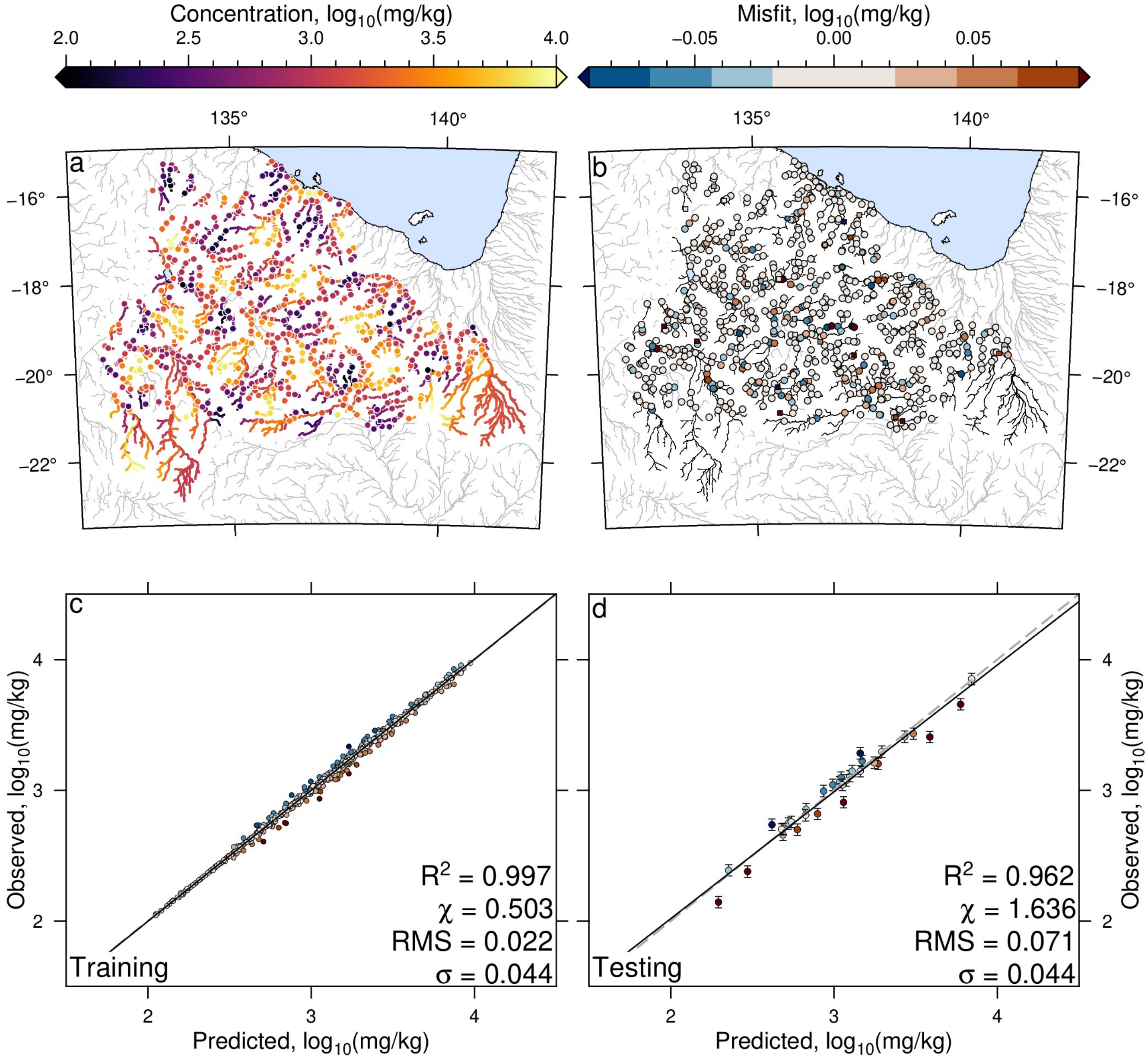

Figure 4: **Inverting synthetic data: evaluating fit to downstream concentrations** a) Coloured lines = predicted downstream concentration for synthetic example. Calculated by using the result in shown in Figure 3 as an input for the forward mixing model (Equation 1); coloured circles = 'observed' synthetic concentrations calculated from synthetic input (Figure 3a) with 10 % added noise; coloured squares = same as coloured circles but for the unseen test dataset; grey lines = channels outside modelled domain. b) Coloured circles = misfit between predicted and 'observed' concentration for training dataset overlain onto modelled channels (black lines); coloured squares = same as coloured circles for test dataset. c) Cross plot of predicted downstream concentration from best fit solution against the 'observed' synthetic training data, coloured by misfit. Error bars are excluded to improve clarity, but displayed at same scale in panel d. Grey dashed line = 1:1 lines; black solid line = regression through data; χ = ratio of root mean square misfit (RMS) to observational uncertainty (σ). d) Same as panel c for unseen downstream test dataset.

We note that the scheme is successful in recovering the expected locations of peaks and troughs across the region. We also identify two regions of poor recovery in the far south west and south east of the study area. These are areas where only a small number of samples were gathered from large sub-catchments. Correspondingly, we have limited ability to resolve any variability within these sub-catchments. As a result, these sub-catchments are set implicitly by the inversion scheme to a constant concentration. The misfit between the expected and recovered map are shown in Figure 3c-d.

Finally we evaluate the accuracy of the downstream predictions (Figure 4). Figure 4a shows the predicted downstream concentration for the recovered upstream map shown in Figure 3b. Overlain on these predictions are the 'observed' synthetic data. Visually we can see a strong similarity reflected in the very small absolute misfit between the predictions and observations (Figure 4b). Plotting the predictions against the observations on a crossplot confirms the good fit with data clustered very tightly to the 1:1 line (Figure 4c). Additionally, we observe that the predicted concentrations also match well against the unseen test dataset (Figure 4d). This result suggests that the recovered model is able to make accurate and unbiased predictions of unseen data. The χ value (ratio of root mean square misfit to expected error) of both training and test data are close to 1 as expected, although higher (and above 1) for the test dataset. This suggests a slight overfitting of the training dataset.

4.1.1 Resolution

By repeating the synthetic test described above with input maps with varying wavelengths we can deduce an effective resolution of our sampling campaign. The resolution of the campaign will be the smallest wavelength pattern that can be reliably recovered. Neglecting the two previously identified blind-spots, we find our scheme is able to resolve features greater than 0.5 - 1° (or ~ 50 – 100 km) in size (see Supplementary Information). This size is two to five times the nominal average distance between NAGS samples.

Whilst we consider only chequerboard tests here, it is possible to investigate the ability of the inverse scheme to recover any proposed signal. For example, whether a geochemical anomaly of a given location, extent and magnitude can be recovered from downstream sediments.

4.2 Inverting real data

Having validated the method using synthetic tests we proceed to generate geochemical maps for all 46 studied elements from the NAGS dataset. We focus herein on two elements, Cu and Nd (a rare earth element), which have potential economic interest in the region. Analogous maps for all other elements are provided in the Supplementary Information.

4.2.1 Copper

The optimal upstream concentration for Cu is shown in Figure 5a. It was generated using a smoothing parameter of $10^{3.5}$. Most of the domain shows a relatively constant concentration around 15 – 25 mg kg^{-1}. However, in the northeast and east of the domain there are regions of significantly elevated predicted concentrations, up to 100 mg kg^{-1}. We note that these locations approximately coincide with a steep gradient in the lithosphere-asthenosphere boundary, which appears to be a strong predictor of Cu and base metal deposits (Hoggard et al. 2020).

By applying the forward, mixing, model to the upstream map shown in Figure 5a we make continuous predictions of elemental concentration in downstream sediments, shown in Figure 5. Crossplots of these downstream predictions, evaluated at the sample sites, against the observed concentrations are shown in Figures 5c & d for the training and test dataset respectively. In both cases the χ value is close to one which indicates a good fit to the data with limited over or underfitting.

We note in Figure 5c that three points (highlighted with a red arrow) have observed concentrations greater than 4 RMS values above the predicted values. The locations of these outlying points are highlighted in Figure 5e, and coincide with the broader regions of high concentration discussed above. One possible explanation is that there is a small localised region of even higher concentration in the sub-catchments upstream of these samples. Due to the constraints imposed by the model smoothing, this small-wavelength anomalies could potentially be unresolvable. Consequently, significantly underpredicted samples could possibly indicate catchments containing anomalously short-wavelength and high-magnitude concentrations.

4.2.2 Neodymium

An analogous map for Nd is shown in Figure 6. In this instance the χ values are larger than one indicating a slight underfit to the data. However, the regression through the test dataset is effectively parallel to the 1:1 line indicating unbiased estimation of downstream data. The map shown in Figure 6a indicates two main regions of elevated Nd concentration. The first is a broad band trending west-northwest to east-southeast in the north of the region. This band runs parallel to the boundary of the Cenozoic basin shown in Figure 2b and also broadly corresponds to the Barkly Tableland geomorphologic feature. The second area of elevated Nd lies in the south of the region centred on 139°E, -21°S. This particular area is discussed at greater length in the Discussion section.

4.3 Comparison to independent survey data

Predictions of sediment geochemistry downstream can also be tested against independent alluvial sediment data gathered as part of the independent and preceding National Geochemical Survey of Australia (NGSA; Caritat et al. 2011; Caritat 2018). This nationwide survey is of a lower density than the one used to invert for source concentrations but contains a number of samples within our study area. In the NGSA both top-soil (0 – 10 cm) and sub-soil (~ 60 – 80 cm) samples were gathered. We show here the comparison against the top-soil data but results are largely the same if sub-soil was used. We compare our data only against the fine (< 75 μm) grain-size fraction, which is identical to the grain-size fraction analysed in the northern Australia study.

Figures 7a & c display cross-plots between predicted and observed Cu and Nd concentrations at the NGSA sample sites. We find the regression between the points to be sub-parallel to 1:1 in both instances which is encouraging. The RMS misfit for both elements relative to NGSA is larger than for the test datasets

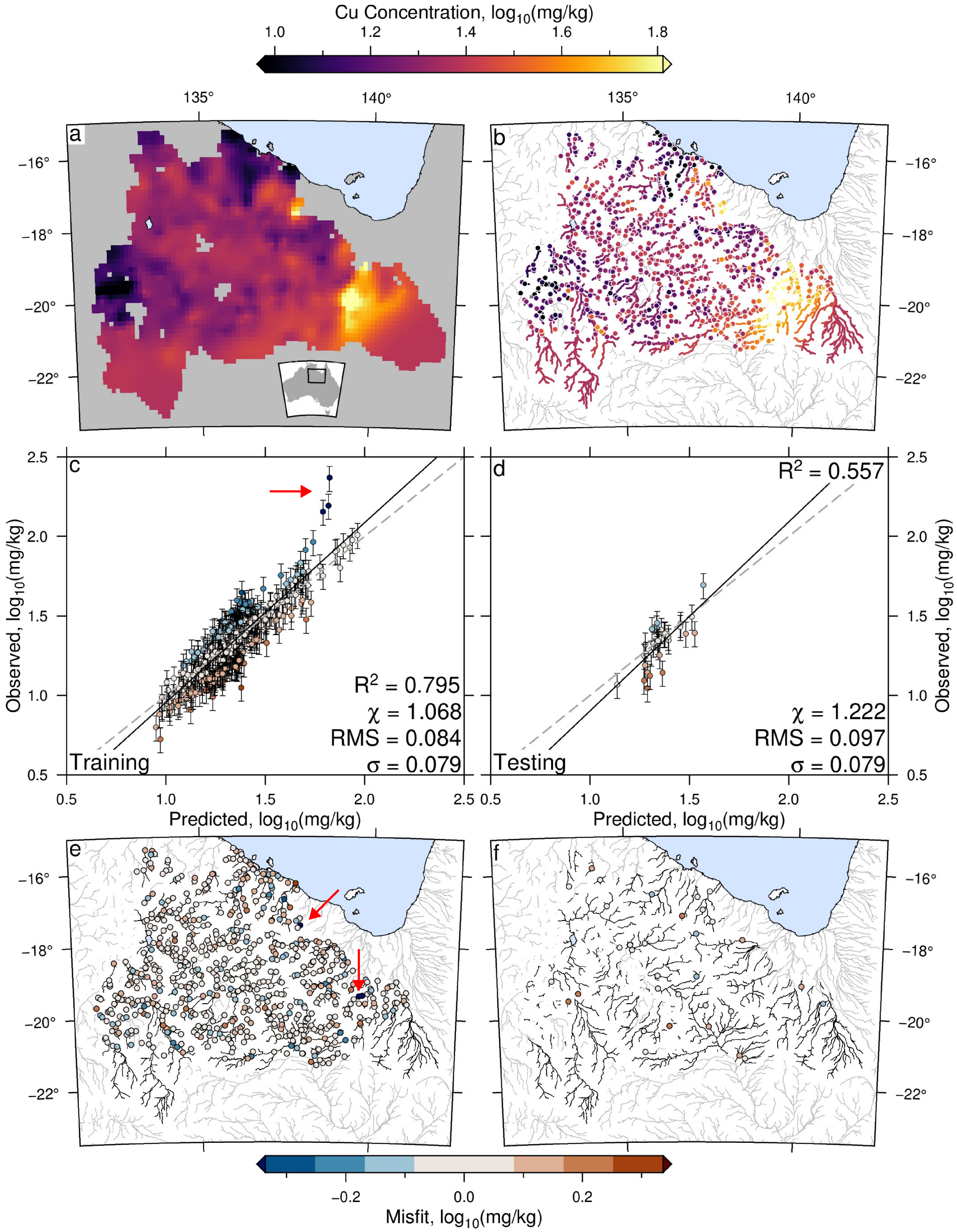

Figure 5: **Inverting for Cu concentrations in northern Australia.** a) Best-fitting upstream concentration map for Cu, generated by minimising Equation 2 with a smoothing parameter of $10^{3.5}$. b) Coloured lines = predicted downstream sediment concentration calculated by entering result shown in panel a) into forward mixing model (Equation 1). coloured circles = observed concentration in training dataset (see panels c & e); coloured squares = same as coloured circles but for test dataset (panels d & f); grey lines = channels outside of covered region. c) Cross plot of observed and predicted concentration at training sample sites. Colour bar (also used in panels d–f) has incremements equal to the RMS of the training dataset. Red arrows highlight underpredicted samples (see also panel e and body text); χ = ratio of RMS misfit to σ; σ = standard deviations. d) Same as panel c for test dataset. e–f) Spatial map of the misfit to testing and training datasets.

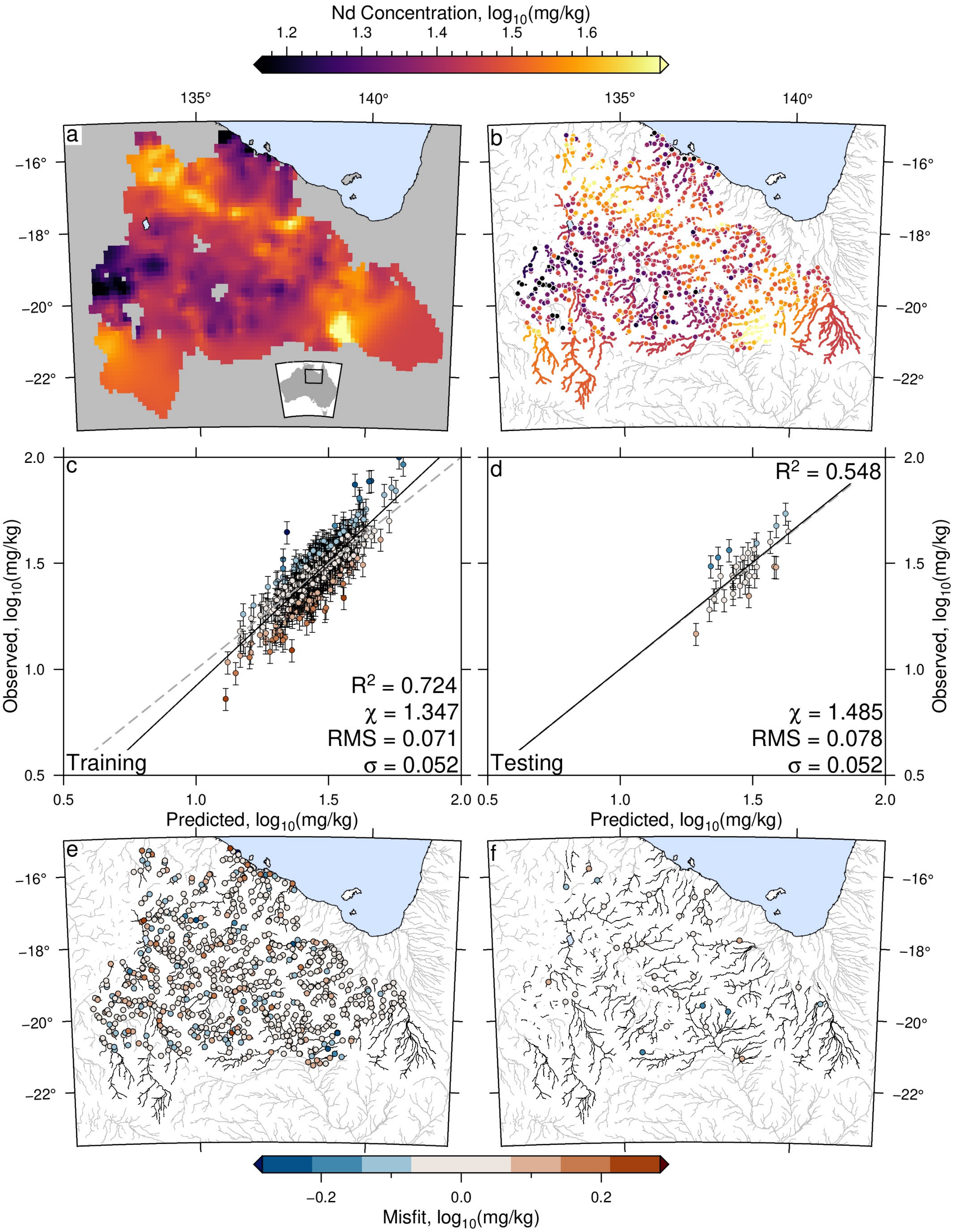

Figure 6: **Inverting for Nd concentrations in northern Australia.** a) Best-fitting upstream concentration map for Nd, generated by minimising Equation 2 with a smoothing parameter of $10^{3.5}$. b) Coloured lines = predicted downstream sediment concentration calculated by entering result shown in panel a) into forward mixing model (Equation 1). Coloured circles = observed concentration in training dataset (see panels c & e); coloured squares = same as coloured circles but for test dataset (panels d & f); grey lines = channels outside of covered region. c) Cross plot of observed and predicted concentration at training sample sites. Colour bar (also used in panels d–f) has increments equal to the RMS of the training dataset. χ = ratio of RMS misfit to σ; σ = standard deviations. d) Same as panel c for test dataset. e) Spatial map of the misfit to testing and training datasets.

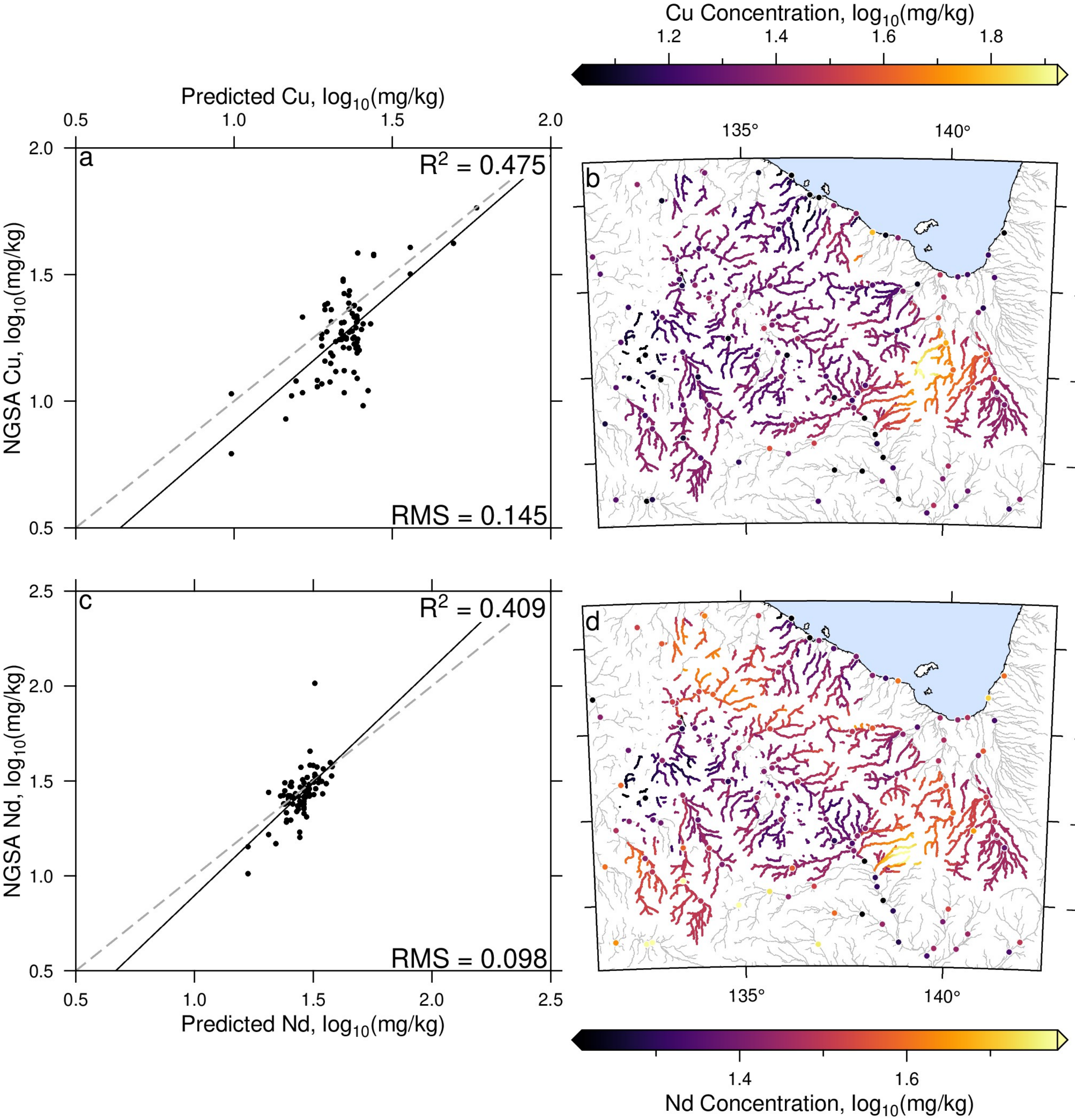

Figure 7: **Comparing predictions from inverse scheme to independent NGSA data.** a) Cross-plot of Cu concentrations in NGSA samples against predicted Cu concentration from this study. Black line = regression through data; grey dashed line = 1:1 line. b) Coloured lines = predicted downstream sediment Cu concentration reproduced from Figure 5b; coloured circles = observed concentration in NGSA dataset; grey lines = channels outside of model coverage. c) Same as panel a but for Nd. d) Same as panel c but for Nd.

shown above, especially for Cu. One possible explanation for this is that no inter-survey levelling has been carried out prior to analysis. The NGSA data for Cu and Nd is shown overlain on the predictions from this study in Figure 7b & d.

4.4 Principal Component Analysis

Whilst individual elemental maps are useful, wider geologic understanding can be gained by extracting information from multiple elements simultaneously (e.g., Grunsky 2010; Caritat and Grunsky 2013; Kirkwood et al. 2016). Here, we use principal component analysis (PCA) to map the significant geochemical domains in the region, shown in Figure 8a. This map was generated by first calculating the first three principal components for the geochemical maps for all analysed elements. The PCA calculation was performed after a centred log-ratio (clr) transformation as geochemical data is compositional in nature (Aitchison 1983). The clr coordinates are not normalised/whitened prior to PCA. These first three components contain 76.0 % of the total variance (individual variances shown on Figure 8c–e). To generate a false-colour composite each of the scores on the first three components were rescaled to range between 0 and 1 and used to weight RGB colour channels. The loadings on each element for each principal component are shown in Figures 8c–e.

The first principal component (PC1, reds), shows strong positive loadings in magnesium (Mg) and calcium (Ca) but negative loadings in zirconium (Zr) and hafnium (Hf). Given that Zr and Hf are frequently found in detrital minerals such as zircon, but Ca and Mg are often found in carbonates, this could indicate a siliciclastic/carbonate distinction. PC2 (green) shows strong positive loadings on rubidium (Rb), barium (Ba), sodium (Na) and potassium (K), all of which are associated with feldspar minerals. PC3 (blue) may be related to enrichment in certain metals showing strong positive loadings in sodium (Na), vanadium (V), cobalt (Co) and Cu, as well as many of the rare earth elements.

By comparing the geochemical domains in Figure 8a to the geological map in Figure 8b we note strong similarities in spatial structure. This result is consistent with the observation that lithology is the first order control on stream and river sediment chemistry (e.g., Everett et al. 2019).

The green-blue domain (loadings in PC2 and PC3) in the North of the region (A in Figure 8a–b) coincides with outcrops of the Paleoproterozoic and Paleozoic sedimentary rocks. This outcrops again to the south-west (D in Figure 8a–b). The Cenozoic cover in the centre of the region between the two Paleoproterozoic outcrops (map unit CZu in Figure 8b) geochemically appears to be made up of (at least) two distinct domains. The first domain shows strong scores in PC1 generating a red-purple band running NE-SW (B in Figure 8a–b). The second domain, to the south, shows a greater loading on PC2 generating an orange band further to the south-west (C in Figure 8a–b). Alternatively, the purple band (B) could represent map unit Ks and the orange unit represent CZu. Both interpretations would require verification in the field. To the south-east of the region (e.g., -20°N, 140°E) all components have high scores, in particular PC3 (E in Figure 8a–b).

5 DISCUSSION

5.1 Sensitivity and Uncertainty

An important result from explicitly considering alluvial sediment as a mixture is that samples from downstream sub-catchments will be less sensitive to changes in their sub-catchment's source chemistry than those further upstream. This change in sensitivity is because, further downstream, each sub-catchment contributes a relatively smaller proportion to the total amount of sediment than further upstream. Consequently, any change in sub-catchment source concentration has a smaller observable impact downstream than it does upstream. For example, in Figure 1, assuming each sub-catchment has equal area, sub-catchment D only contributes one quarter of the sediment to observation point D. By contrast, at sample site A, sub-catchment A contributes all of the material. As a result, to have the same observable impact on sediment chemistry as at site A, any change in chemistry of sub-catchment D would have to be four times larger.

A compounding effect is that the composition of upstream sub-catchments are also constrained by samples further downstream whilst downstream sub-catchments are not. For example, in Figure 1, the concentration in sub-catchment A is constrained at site A, but also by site C and D. In contrast, sub-catchment D is only constrained by site D. Consequently the uncertainty on source predictions may be lower than the analytical uncertainty of the individual observations. By contrast, the uncertainty on the predicted source concentrations for the most downstream sub-catchments may be greater than the uncertainty on the individual measurements. Note, these general and simple heuristics neglect the effects of the regulariser.

5.2 Comparison to Kriging

Here we discuss, using synthetic and real results, how the results form the inversion method presented in this study compare to the more commonly used geostatistical technique of kriging.

5.2.1 Synthetic tests

We first investigate how kriging performs in the synthetic test described in Section 4.1. There, we demonstrated how our inversion scheme successfully recovered a synthetic chequerboard input geochemical map (Figure 3) even when noise was added to the synthetic 'observations'. We now apply kriging to these same 'observations' to see if kriging too can recover the input map. The results of this experiment are shown in Figure 9. We find that the kriged map (Figure 3c) is significantly dampened relative to the true expected solution (Figure 3a). This result contrasts with the unmixed solution which correctly recovers the magnitude of the variability (Figure 3b). Not only is the magnitude of the solution not recovered, the spatial structure of the solution is also distorted (Figure 9d). The synthetic input consisted of regular and symmetrical peaks/troughs of concentration. This pattern is notably distorted in the kriged map.

Consequently, we conclude that kriging fails to adequately recover synthetic geochemical maps from downstream samples. By contrast, the inverse scheme presented in this study can recover such inputs.

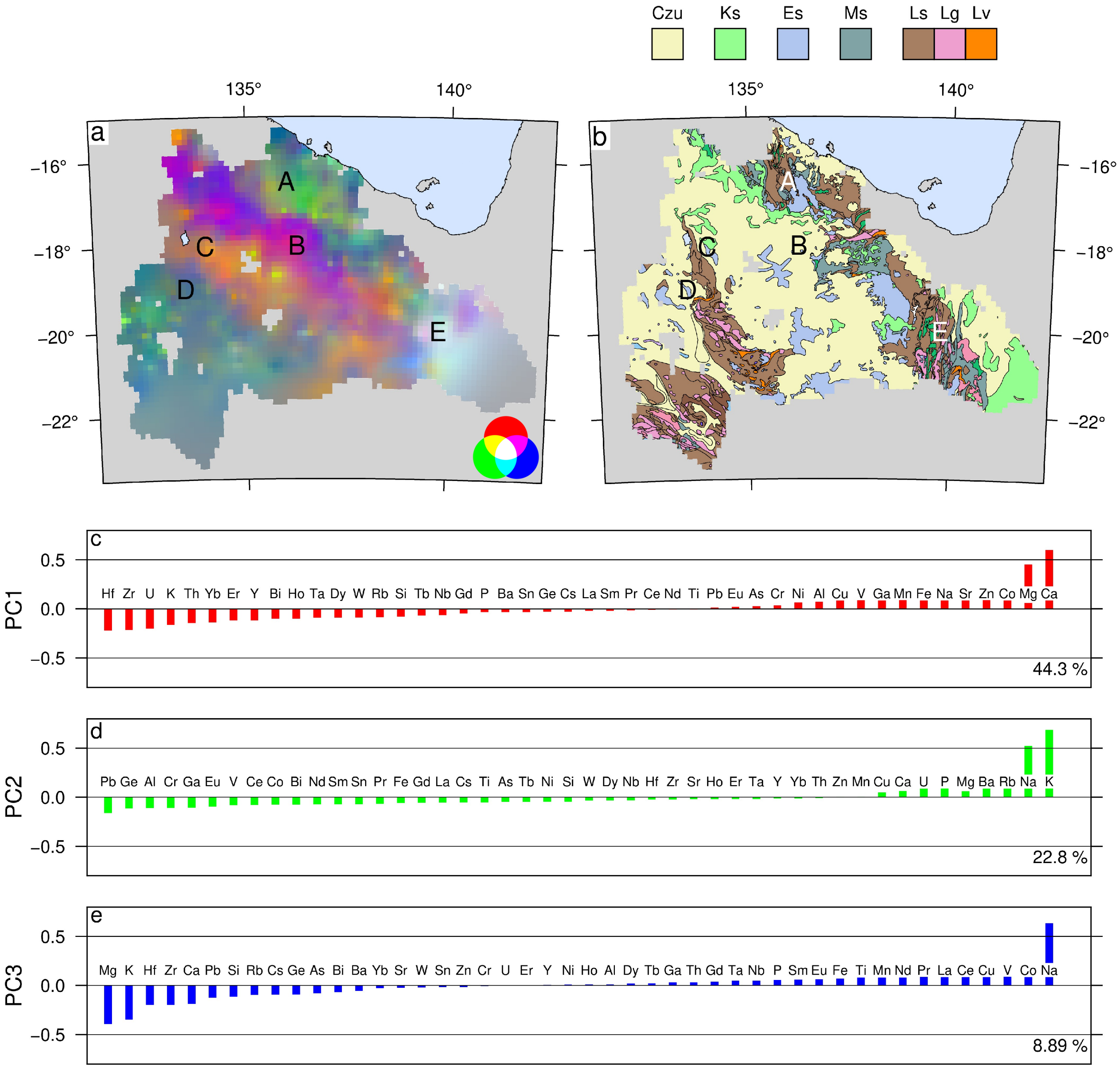

Figure 8: **Principal geochemical domains of northern Australia calculated using principal component analysis.** a) First three principal components of 46 elemental upstream prediction maps. First, second and third components passed respectively to red, green and blue (RGB) colour channels to generate false colour composite. Scandium is excluded due to spurious variance introduced by imputation. Inset shows additive mixing of RGB colourbands. Letters A – E highlight different geochemical domains discussed in the body-text. b) 1:1 million scale geological map of Australia (Raymond et al. 2012). Colours for selected lithologies shown: CZu = Cenozoic sediments; Ks = Cretaceous sediments; Es = Cambrian sediments; Ms = Mesoproterozoic sediments; Ls = Paleoproterozoic sediments; Lg = Paleoproterozoic felsic intrusives; Lv = Paleoproterozoic intermediate volcanics; see original source for full legend. Reproduced from Figure 2b. c) First principal component loadings on each (clr transformed) element in dataset. The proportion of total variance contained on this component is given in the lower right of the panel. d) Same as panel c for second principal component. e) Same as panel c for third principal component.

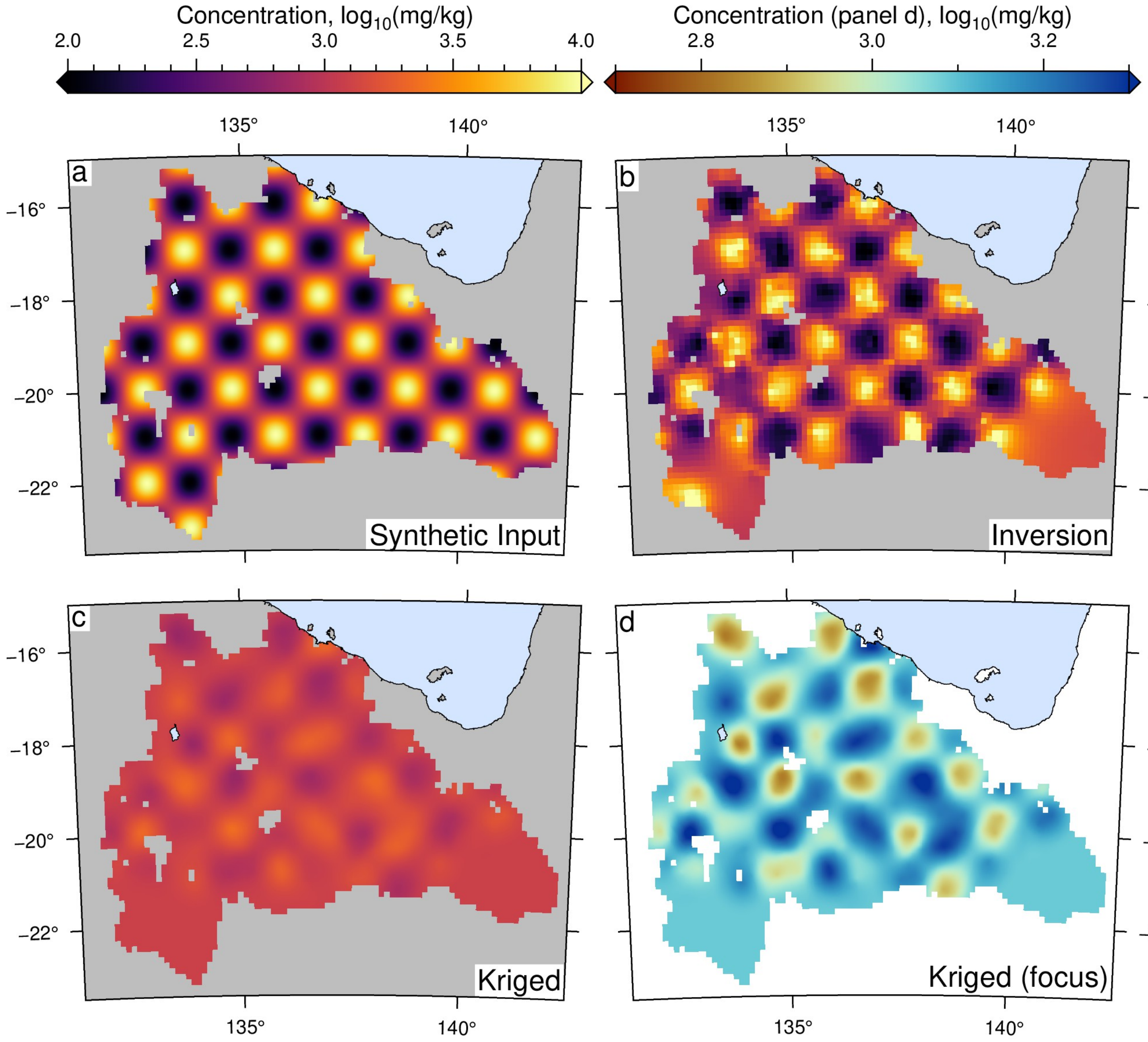

Figure 9: **Recovering a synthetic geochemical map through kriging.** a) Synthetic geochemical map which we seek to recover (Figure 3a). Sinusoidal variations in concentration with spatial wavelength of 2° between 10^2 and 10^4 mg kg^{-1}. b) Input recovered using the inverse/unmixing method described in this study (Figure 3b). c) Geochemical map generated by applying kriging (spherical variogram) to the same log-transformed synthetic 'observations' data as used for panel b. Note that this uses the same colour-scale as panels a and b. d) Same as panel c but using a colour-scale focussed on the range of the kriged predictions.

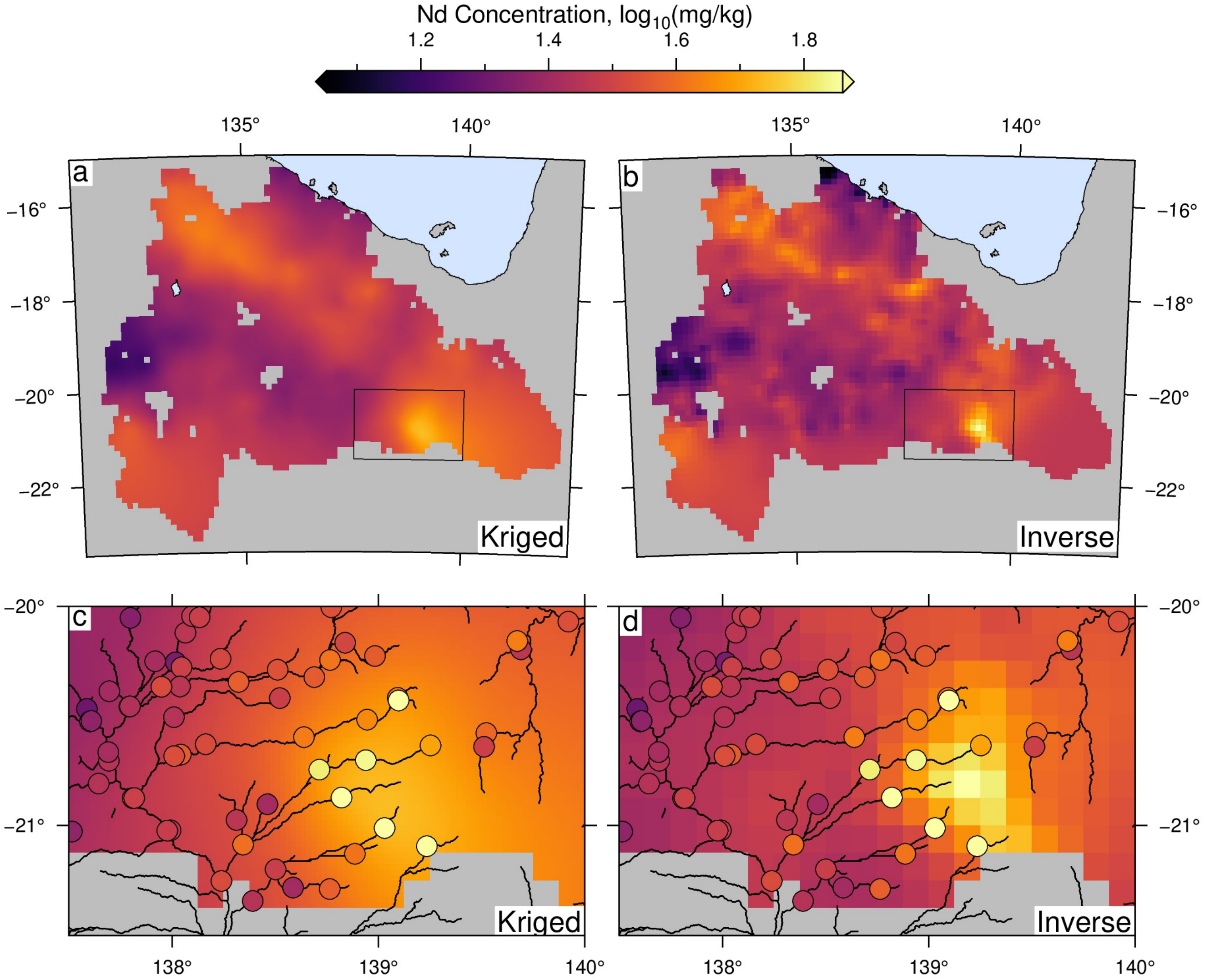

Figure 10: **Comparing the inverse scheme to kriging.** a) Map of Neodymimum concentrations over study region generated by applying ordinairy kriging to the (log transformed) NAGS dataset. Square indicates the location of the areas shown in panels c–d. b) Map of Nd concentrations over study region generated by the inverse methodology presented in this study. c) Focussed view of area outlined in panel a. Black lines = river channels. Coloured circles = Observed Nd concentrations from NAGS dataset. d) Same as for panel c but showing a focussed view of the inverse prediction shown in panel a. Note that panels c–d use a Mercator projection.

5.2.2 *Real data*

We now discuss the geochemical maps for Nd, generated using both these techniques (Figure 10). The kriged map displayed here was generated through ordinary kriging, applied to the log-transformed data, assuming a spherical variogram. Whilst we focus on kriging here, the discussion also largely applies to other geostatistical methods that do not consider hydrological structure (e.g., a tensioned spline; Smith and Wessel 1990).

Whilst the larger-scale structures are superficially similar (e.g., Figures 10a–b) we note that the kriged map shows variations in concentration of a lower amplitude. There are more significant differences on smaller length-scales. These differences are introduced because kriging (and other geostatistical methods) do not consider the importance of topological distance when interpolating. An illustrative example is shown in Figures 10c–d, centred around a region of samples with high Nd concentrations. Kriging simply centres the region of elevated concentration on the sample localities themselves (Figure 10c). However, the unmixing scheme, correctly, identifies that the source of elevated Nd does not necessarily need to align with the samples of high concentration, simply to be *upstream* of them. This logic is more consistent with the fact that stream sediments are mixtures of their upstream basins. Additionally, we note that for this particular area, the kriged map is significantly more dampened than the inverse map, displaying a broader and shallower feature. Hence, kriging can generate geochemical anomalies with both different magnitude and locations to those calculated by our unmixing method. Given the failure of kriging to recover synthetic inputs, it seems likely that maps generated through unmixing are more reliable. This result has significant implications if kriged maps are subsequently used for establishing environmental baselines or for prospectivity mapping.

6 CONCLUSIONS

We presented a demonstration of how regional alluvial geochemical survey data can be unmixed to generate continuous geochemical maps of sediment source regions. Synthetic data, combined with our approach, can be used to investigate the ability of geochemical surveys to recover theoretical geochemical features in the study region. Using real data gathered as part of the Northern Australia Geochemical Survey we have produced continuous maps of 46 elements. These geochemical maps compare favourably against an unseen sub-set of the survey data as well as data from an independent geochemical survey. We find that kriging, which does not consider hydrological structure, can produce geochemical maps that, especially on short wavelengths, have significant differences to mapped concentrations. Such differences could result in geochemical anomalies being mislocated or mapped with different magnitudes. We argue that the unmixing method is an appropriate way to use alluvial geochemical data to generate reliable continuous geochemical maps.

DATA AND CODE AVAILABILITY

A data and code repository for this manuscript can be found archived at `doi.org/10.5281/zenodo.7108427`. These repositories contain 1) a minimum working example of the unmixing scheme is provided as a python script and an annotated python Jupyter Notebook; 2) data required to reproduce our results and 3) ASCII grid files of all generated geochemical maps.

SUPPLEMENTARY INFORMATION

The Supplementary Information document is not presented here due to its size but is available upon request to the author. Alternatively, it will be made available upon journal publication.

ACKNOWLEDGEMENTS

AGL acknowledges funding from NERC SSCP DTP grant code NE/L002515/1. The Northern Australia Geochemical Survey and the National Geochemical Survey of Australia were funded by the Australian Government's Exploring for the Future and Onshore Energy Security programmes, respectively. We acknowledge the traditional custodians of the lands on which these samples were collected, and thank all landowners for granting access to the sampling sites. PdC publishes with the permission of the Chief Executive Officer of Geoscience Australia.

REFERENCES

Ahmad, M. and I. R. Scrimgeour (2013). "Chapter 2: Geological framework". In: *Geology and mineral resources of the Northern Territory*. Special Publications 5. Northern Territory Geological Survey.

Aitchison, J. (1983). "Principal component analysis of compositional data". *Biometrika* 70.1, pp. 57–65. DOI: `10.1093/biomet/70.1.57`.

Bastrakov, E. N., P. Main, A. Wygralak, J. Wilford, K. Czarnota, and M. Khan (2018). *Northern Australia Geochemical Survey: Data release 1 - Total (fine fraction) and MMI™ element contents*. Geoscience Australia. DOI: `10.11636/Record.2018.006`.

Betts, P. G., D. Giles, G. S. Lister, and L. R. Frick (2002). "Evolution of the Australian lithosphere". *Australian Journal of Earth Sciences* 49.4, pp. 661–695. DOI: `10.1046/j.1440-0952.2002.00948.x`.

Birke, M., U. Rauch, and J. Stummeyer (2015). "How robust are geochemical patterns? A comparison of low and high sample density geochemical mapping in Germany". *Journal of Geochemical Exploration* 154, pp. 105–128. DOI: `10.1016/j.gexplo.2014.12.005`.

Blewett, R. (2012). *Shaping a Nation*. ANU Press. DOI: `10.22459/SN.08.2012`.

Bølviken, B., J. Bogen, M. Jartun, M. Langedal, R. T. Ottesen, and T. Volden (2004). "Overbank sediments : a natural bed blending sampling medium for large—scale geochemical mapping". *Chemometrics and Intelligent Laboratory Systems*. Special Issue: 50 years of Pierre Gy's Theory of Sampling Proceedings: First World Conference on Sampling and Blending (WCSB1) Tutorials on sampling: Theory and Practice 74.1, pp. 183–199. DOI: `10.1016/j.chemolab.2004.06.006`.

Bonham-Carter, G. and W. Goodfellow (1986). "Background corrections to stream geochemical data using digitized drainage and geological maps: application to selwyn basin, yukon and northwest territories". *Journal of Geochemical Exploration* 25.1, pp. 139–155. DOI: `10.1016/0375-6742(86)90011-7`.

Braun, J., J. Dooley, B. Goleby, R. van der Hilst, and C. Klootwijk (1998). *Structure and Evolution of the Australian Continent*. Geodynamics Series 26. American Geophysical Union.

Braun, J. and S. D. Willett (2013). "A very efficient O(n), implicit and parallel method to solve the stream power equation governing fluvial incision and landscape evolution". *Geomorphology* 180-181, pp. 170–179. doi: 10.1016/j.geomorph.2012.10.008.

Caritat, P. d. and M. Cooper (2016). "A continental-scale geochemical atlas for resource exploration and environmental management: the National Geochemical Survey of Australia". *Geochemistry: Exploration, Environment, Analysis* 16.1, pp. 3–13. doi: 10.1144/geochem2014-322.

Caritat, P. de and E. C. Grunsky (2013). "Defining element associations and inferring geological processes from total element concentrations in Australian catchment outlet sediments: Multivariate analysis of continental-scale geochemical data". *Applied Geochemistry* 33, pp. 104–126. doi: 10.1016/j.apgeochem.2013.02.005.

Caritat, P. d. (2018). "Continental-scale geochemical surveys and mineral prospectivity: Comparison of a trivariate and a multivariate approach". *Journal of Geochemical Exploration* 188, pp. 87–94. doi: 10.1016/j.gexplo.2018.01.014.

Caritat, P. d., M. Cooper, and Geoscience Australia (2011). *National Geochemical Survey of Australia: data quality assessment*. Canberra: Geoscience Australia.

Carranza, E. J. M. (2010). "Mapping of anomalies in continuous and discrete fields of stream sediment geochemical landscapes". *Geochemistry: Exploration, Environment, Analysis* 10.2, pp. 171–187. doi: 10.1144/1467-7873/09-223.

Carranza, E. J. M. and M. Hale (1997). "A catchment basin approach to the analysis of reconnaissance geochemical-geological data from Albay Province, Philippines". *Journal of Geochemical Exploration* 60.2, pp. 157–171. doi: 10.1016/S0375-6742(97)00032-0.

Clark, A. D., L. J. Morrissey, M. P. Doublier, N. Kositcin, A. Schofield, and R. G. Skirrow (2022). "A newly recognised 1860–1840 Ma tectono-magmatic domain in the North Australia Craton: Insights from the Tennant Region, East Tennant area, and the Murphy Inlier". *Precambrian Research* 375, p. 106652. doi: 10.1016/j.precamres.2022.106652.

Ercolani, C., D. Lemarchand, and A. Dosseto (2019). "Insights on catchment-wide weathering regimes from boron isotopes in riverine material". *Geochimica et Cosmochimica Acta*. doi: 10.1016/j.gca.2019.07.002.

Everett, P., A. Donald, A. Ferreira, F. Fordyce, C. Gowing, R. Lawley, T. Lister, B. Palumbo-Roe, and British Geological Survey (2019). *Stream sediment geochemical atlas of the United Kingdom: British Geological Survey report OR/18/048*. British Geological Survey.

Gao, F. and L. Han (2012). "Implementing the Nelder-Mead simplex algorithm with adaptive parameters". *Computational Optimization and Applications* 51.1, pp. 259–277. doi: 10.1007/s10589-010-9329-3.

Garrett, R., C. Reimann, D. Smith, and X. Xie (2008). "From geochemical prospecting to international geochemical mapping: a historical overview". *Geochemistry: Exploration, Environment, Analysis* 8.3, pp. 205–217. doi: 10.1144/1467-7873/08-174.

Grunsky, E. C. (2010). "The interpretation of geochemical survey data". *Geochemistry: Exploration, Environment, Analysis* 10.1, pp. 27–74. doi: 10.1144/1467-7873/09-210.

Hoggard, M. J., K. Czarnota, F. D. Richards, D. L. Huston, A. L. Jaques, and S. Ghelichkhan (2020). "Global distribution of sediment-hosted metals controlled by craton edge stability". *Nature Geoscience* 13.7, pp. 504–510. doi: 10.1038/s41561-020-0593-2.

Hutchinson, M. F., J. L. Stein, J. A. Stein, H. Anderson, and P. K. Tickle (2008). *GEODATA 9 Second DEM and D8 digital elevation model version 3 and flow direction grid 2008*. Canberra, ACT: Geoscience Australia.

Isbell, R. F. (2016). *The Australian soil classification*. In collab. with N. C. on Soil {and} Terrain (Australia). Second edition. Australian soil and land survey handbooks series volume 4. Clayton South, Victoria: CSIRO Publishing. 141 pp.

Johnson, C. C., N. Breward, E. L. Ander, and L. Ault (2005). "G-BASE: baseline geochemical mapping of Great Britain and Northern Ireland". *Geochemistry: Exploration, Environment, Analysis* 5.4, pp. 347–357. doi: 10.1144/1467-7873/05-070.

Kim, S.-T. and J. R. O'Neil (1997). "Equilibrium and nonequilibrium oxygen isotope effects in synthetic carbonates". *Geochimica et Cosmochimica Acta* 61.16, pp. 3461–3475. doi: 10.1016/S0016-7037(97)00169-5.

Kirkwood, C., P. Everett, A. Ferreira, and B. Lister (2016). "Stream sediment geochemistry as a tool for enhancing geological understanding: An overview of new data from south west England". *Journal of Geochemical Exploration* 163, pp. 28–40. doi: 10.1016/j.gexplo.2016.01.010.

Lipp, A. G., G. G. Roberts, A. C. Whittaker, C. J. B. Gowing, and V. M. Fernandes (2020). "River Sediment Geochemistry as a Conservative Mixture of Source Regions: Observations and Predictions From the Cairngorms, UK". *Journal of Geophysical Research: Earth Surface* 125.12, e2020JF005700. doi: https://doi.org/10.1029/2020JF005700.

– (2021). "Source Region Geochemistry From Unmixing Downstream Sedimentary Elemental Compositions". *Geochemistry, Geophysics, Geosystems* 22.10, e2021GC009838. doi: 10.1029/2021GC009838.

Liu, D., X. Wang, L. Nie, H. Liu, B. Zhang, and W. Wang (2021). "Comparison of geochemical patterns from different sampling density geochemical mapping in Altay, Xinjiang Province, China". *Journal of Geochemical Exploration*, p. 106761. doi: 10.1016/j.gexplo.2021.106761.

Moon, C. J. (1999). "Towards a quantitative model of downstream dilution of point source geochemical anomalies". *Journal of Geochemical Exploration* 65.2, pp. 111–132. doi: 10.1016/S0375-6742(98)00065-X.

Northcote, K. H., G. G. Beckmann, E. Bettenay, H. M. Churchward, D. C. Van Dijk, G. M. Dimmock, G. D. Hubble, R. F. Isbell, W. M. McArthur, G. G. Murtha, K. D. Nicolls, T. R. Paton, C. H. Thompson, A. A. Webb, and M. J. Wright (1968). *Atlas of Australian Soils, Sheets 1 to 10. With explanatory data*. Melbourne: CSIRO Australia and Melbourne University Press.

O'Callaghan, J. F. and D. M. Mark (1984). "The extraction of drainage networks from digital elevation data". *Computer Vision, Graphics, and Image Processing* 28.3, pp. 323–344. doi: 10.1016/S0734-189X(84)80011-0.

Ollier, C. D. (1988). “The regolith in Australia”. *Earth-Science Reviews* 25.5, pp. 355–361. DOI: 10.1016/0012-8252(88)90003-7.

Ottesen, R. T., J. Bogen, B. Bølviken, and T. Volden (1989). “Overbank sediment: a representative sample medium for regional geochemical mapping”. *Journal of Geochemical Exploration*. 12th International Geochemical Exploration Symposium and the 4th Symposium on Methods of Geochemical Prospecting 32.1, pp. 257–277. DOI: 10.1016/0375-6742(89)90061-7.

Pain, C., L. Gregory, P. Wilson, and N. McKenzie (2011). “The physiographic regions of Australia. Explanatory notes”. *Australian Collaborative Land Evaluation Program*.

Press, W. H., S. A. Teukolsky, W. T. Vetterling, and B. P. Flannery (1992). *Numerical Recipes in FORTRAN: The Art of Scientific Computing*. 2nd ed. New York, NY: Cambridge University Press.

Rawlinson, N., A. Fichtner, M. Sambridge, and M. K. Young (2014). “Seismic Tomography and the Assessment of Uncertainty”. In: *Advances in Geophysics*. Vol. 55. Elsevier, pp. 1–76. DOI: 10.1016/bs.agph.2014.08.001.

Raymond, O. L., S. Liu, R. Gallagher, W. Zhang, and L. M. Highet (2012). *Surface Geology of Australia 1:1 million scale dataset*. Canberra, ACT: Geoscience Australia.

Rodriguez-Galiano, V., M. Sanchez-Castillo, M. Chica-Olmo, and M. Chica-Rivas (2015). “Machine learning predictive models for mineral prospectivity: An evaluation of neural networks, random forest, regression trees and support vector machines”. *Ore Geology Reviews* 71, pp. 804–818. DOI: 10.1016/j.oregeorev.2015.01.001.

Salminen, R., M. J. Batista, M. Bidovec, A. Demetriades, B. D. Vivo, W. D. Vos, M. Duris, A. Gilucis, V. Gregorauskiene, J. Halamic, P. Heitzmann, A. Lima, G. Jordan, G. Klaver, P. Klein, J. Lis, J. Locutura, K. Marsina, A. Mazreku, P. J. O’Connor, S. A. Olsson, R.-T. Ottesen, V. Petersell, J. A. Plant, S. Reeder, I. Salpeteur, H. Sandström, U. Siewers, A. Steenfelt, and T. Tarvainen (2005). *Geochemical Atlas of Europe. Part 1: Background Information, Methodology and maps*. Geological Survey of Finland.

Senior, A., A. Britt, D. Summerfield, A. Hughes, A. Hitchman, A. Cross, D. Champion, D. Huston, E. Bastrakov, M. Sexton, J. Maloney, J. Pheeney, M. Teh, and A. Schofield (2021). *Australia’s indentified mineral resources 2020*. Geoscience Australia. DOI: 10.11636/1327-1466.2020.

Smith, D. B. and C. Reimann (2008). “Low-density geochemical mapping and the robustness of geochemical patterns”. *Geochemistry: Exploration, Environment, Analysis* 8.3, pp. 219–227. DOI: 10.1144/1467-7873/08-171.

Smith, W. H. F. and P. Wessel (1990). “Gridding with continuous curvature splines in tension”. *Geophysics* 55.3, pp. 293–305. DOI: 10.1190/1.1442837.

Spadoni, M., G. Cavarretta, and A. Patera (2004). “Cartographic techniques for mapping the geochemical data of stream sediments: the “Sample Catchment Basin” approach”. *Environmental Geology* 45.5, pp. 593–599. DOI: 10.1007/s00254-003-0926-7.

Spadoni, M. (2006). “Geochemical mapping using a geomorphologic approach based on catchments”. *Journal of Geochemical Exploration* 90.3, pp. 183–196. DOI: 10.1016/j.gexplo.2005.12.001.

Vicente, V. A. S., J. A. M. S. Pratas, F. C. M. Santos, M. M. V. G. Silva, P. J. C. Favas, and L. E. N. Conde (2020). “Geochemical anomalies from a survey of stream sediments in the Maquelab Area (Oecussi, Timor-Leste) and their bearing on the identification of mafic-ultramafic chromite rich complex”. *Applied Geochemistry*, p. 104868. DOI: 10.1016/j.apgeochem.2020.104868.

Virtanen, P., R. Gommers, T. E. Oliphant, M. Haberland, T. Reddy, D. Cournapeau, E. Burovski, P. Peterson, W. Weckesser, J. Bright, S. J. van der Walt, M. Brett, J. Wilson, K. J. Millman, N. Mayorov, A. R. J. Nelson, E. Jones, R. Kern, E. Larson, C. J. Carey, I. Polat, Y. Feng, E. W. Moore, J. VanderPlas, D. Laxalde, J. Perktold, R. Cimrman, I. Henriksen, E. A. Quintero, C. R. Harris, A. M. Archibald, A. H. Ribeiro, F. Pedregosa, and P. van Mulbregt (2020). “SciPy 1.0: fundamental algorithms for scientific computing in Python”. *Nature Methods* 17.3, pp. 261–272. DOI: 10.1038/s41592-019-0686-2.

Wang, X., X. Liu, and W. Wang (2022). “National-scale distribution and its influence factors of calcium concentrations in Chinese soils from the China Global Baselines project”. *Journal of Geochemical Exploration* 233, p. 106907. DOI: 10.1016/j.gexplo.2021.106907.

Wang, X., B. Zhang, L. Nie, W. Wang, J. Zhou, S. Xu, Q. Chi, D. Liu, H. Liu, Z. Han, Q. Liu, M. Tian, B. Zhang, H. Wu, R. Li, Q. Hu, T. Yan, and Y. Gao (2020). “Mapping Chemical Earth Program: Progress and challenge”. *Journal of Geochemical Exploration* 217, p. 106578. DOI: 10.1016/j.gexplo.2020.106578.

Wessel, P., J. F. Luis, L. Uieda, R. Scharroo, F. Wobbe, W. H. F. Smith, and D. Tian (2019). “The Generic Mapping Tools Version 6”. *Geochemistry, Geophysics, Geosystems* 20.11, pp. 5556–5564. DOI: https://doi.org/10.1029/2019GC008515.

Withnall, I. W., L. J. Hutton, R. J. Armit, P. G. Betts, R. S. Blewett, D. C. Champion, and P. A. Jell (2012). “North Australian Craton”. In: *Geology of Queensland*. Brisbane: Geological Survey of Queensland, pp. 23–112.

Xie, X. and H. Cheng (1997). “The suitability of floodplain sediment as a global sampling medium: evidence from China”. *Journal of Geochemical Exploration*. Geochemical Exploration 1995, II 58.1, pp. 51–62. DOI: 10.1016/S0375-6742(96)00051-9.

Yousefi, M., E. J. M. Carranza, and A. Kamkar-Rouhani (2013). “Weighted drainage catchment basin mapping of geochemical anomalies using stream sediment data for mineral potential modeling”. *Journal of Geochemical Exploration* 128, pp. 88–96. DOI: 10.1016/j.gexplo.2013.01.013.

Zhao, G., F. He, X. Dai, S. Zhang, and R. Yu (2014). “Ultra-low density geochemical mapping in Zimbabwe”. *Journal of Geochemical Exploration*. Mining vs. Environment in Africa 144, pp. 552–571. DOI: 10.1016/j.gexplo.2013.11.001.